Supplementary Information for

Interferometric spectroscopy and high-speed orientation detection of individual gold nanorods

Zhixing He[a], *Chengshaui Li*[b], *Hans D. Robinson*[a], *and Yizheng Zhu*[*b]

[a]Department of Physics, Virginia Tech, Blacksburg, VA 24061

[b]Bradley Dept. of Electrical and Computer Engineering, Virginia Tech, Blacksburg, VA 24061

* yizhu1@vt.edu

Scattered field from GNR in the focal plane

As in the main paper, consider gold nanorods with their principal axes aligned with xyz, so that the polarizability tensor is diagonal with the principal values $\{\alpha_1, \alpha_2, \alpha_2\}$ [1]. It is convenient to resolve the amplitude of the incident electric field E_{0i}, which lies in the xy-plane, into components parallel $E_{0//i}$ and perpendicular $E_{0\perp i}$ to the scattering plane, as shown in Fig. S1. The relationship between scattered and incident field can be expressed using the amplitude scattering matrix[1] S as

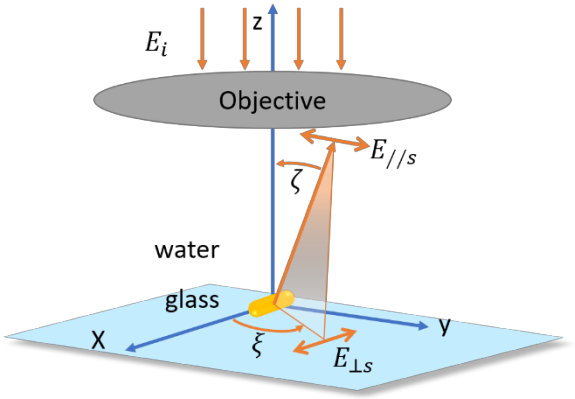

Fig. S1.: *Schematic showing the definitions of quantities used in scattered field calculation.*

$$\begin{pmatrix} E_{//s} \\ E_{\perp s} \end{pmatrix} = \frac{e^{ikr}}{-ikr} \begin{pmatrix} S_2 & S_3 \\ S_4 & S_1 \end{pmatrix} \begin{pmatrix} E_{0//i} \\ E_{0\perp i} \end{pmatrix}, \tag{S1}$$

where the scattered field is uniformly divergent in the far field (kr is large). If we assume that the particle is small compared to the wavelength of light, i.e. that the quasi-static approximation

applies, and recall that the particle is aligned with the coordinate system, the elements of the amplitude scattering matrix can be simplified to

$$\begin{aligned} S_1 &= \frac{-ik^3}{4\pi}(\alpha_1 \sin^2\xi + \alpha_2 \cos^2\xi) \\ S_2 &= \frac{-ik^3}{4\pi}\cos\zeta(\alpha_1 \cos^2\xi + \alpha_2 \sin^2\xi) \\ S_3 &= \frac{-ik^3}{4\pi}\cos\zeta(\alpha_1 - \alpha_2)\sin\xi\cos\xi \\ S_4 &= \frac{-ik^3}{4\pi}(\alpha_1 - \alpha_2)\sin\xi\cos\xi \end{aligned} . \quad \text{(S2)}$$

with scattering polar angle ξ and scattering azimuthal angle ζ indicating the direction of the scattered light as defined in Fig. S1.

Placing the particle at the focal plane of a lens, whose optical axis is aligned with the incident direction (z), we can study the scattered field in the Fourier plane of the lens. For a focused incident beam polarized along x, its Fourier space field is also a plane with x polarization. The parallel and perpendicular components of the incident field with polarization along the x axis can be expressed as $\begin{pmatrix} E_{0//i} \\ E_{0\perp i} \end{pmatrix} = \begin{pmatrix} \cos\xi \\ \sin\xi \end{pmatrix} E_0^c$, where E_0^c is the field amplitude at the beam center where the particle is located. If we approximate the incident light prior to the microscope objective as a plane wave with uniform field amplitude E_0, the optical field amplitude distribution E_f at the focal plane can be calculated using the Fraunhofer approximation as

$$E_f(r_f) = e^{ikf_L} e^{i\frac{kr_f^2}{2f_L}} \frac{kD^2}{i8f_L} E_0 \frac{2J_1(kDr_f/2f_L)}{kDr_f/2f_L}, \quad \text{(S3)}$$

where r_f denotes the distance from the axis within the focal plane, f_L is the focal length of the microscope objective, D is the circular aperture diameter of the focusing lens, and J_1 is the Bessel

function of the first kind. Thus the relationship between E_0^c and E_0 is $\eta = \frac{E_0^c}{E_0} = \frac{kD^2}{8f_L^2} = \frac{1}{2}\left(\frac{NA}{n}\right)^2$, where NA is the numerical aperture of the objective and n is the refractive index of the medium surrounding the nanoparticle (water in our case).

We then obtain:

$$\begin{pmatrix} E_s^x \\ E_s^y \end{pmatrix} = \begin{pmatrix} \cos\xi & \sin\xi \\ \sin\xi & -\cos\xi \end{pmatrix} \begin{pmatrix} E_{//s} \\ E_{\perp s} \end{pmatrix}, \tag{S4}$$

and combining with Eq. (S1), the scattered field in the objective's Fourier plane can be shown to equal

$$\begin{aligned} E_s^x &= \frac{e^{ikr}}{r}\frac{k^2}{4\pi} E_0^c \alpha_1 (\sin^2\xi + \cos^2\xi \cos\zeta) \\ E_s^y &= \frac{e^{ikr}}{r}\frac{k^2}{4\pi} E_0^c \alpha_1 \sin\xi \cos\xi \,(\cos\zeta - 1) \end{aligned}. \tag{S5}$$

It can be seen from this expression that the majority of the power is in the x component. The y component is small, particularly for small ζ. Regardless, due to the y component being anti-symmetric about the x and y axes with respect to ξ, the y component will not be coupled into the rotationally symmetric fundamental mode of the single mode fiber, and thus can be ignored. The scattered field for an anisotropic nanoparticle on the focal plane reduces to

$$E_s = \frac{e^{ikr}}{kr} \kappa E_0 \alpha_1, \tag{S6}$$

where the coupling efficiency κ is given by

$$\begin{aligned} \kappa &\approx \frac{k^3}{4\pi}\frac{\eta}{A}\int_0^{\zeta_{NA}}\int_0^{\pi/2} f(\xi,\zeta)\, r^2 \sin\xi \, d\zeta d\xi \\ A &= 2\pi r^2 (1 - \cos\xi_{NA}) \end{aligned} \tag{S7}$$

as in the main paper, where $f(\xi,\zeta)=\beta(\sin^2\xi+\cos^2\xi\cos\zeta)$. β is a coefficient that accounts for the detection efficiency of the optical system.

The beam measured in the far field or at the detector is a combination of the reflected field from the substrate and the scattered field from the particle. Under the far field approximation, the incident field can be expressed in spherical wave form as $E_{\text{inc}}=\frac{e^{ikr}}{kr}E_0e^{-i\pi/2}$, where r is the distance and the $\pi/2$ phase term comes from the Gouy phase shift [2].

Taking only first order of reflection and scattering into consideration, the total combined field under the first-order Born approximation is

$$E_{\text{ret}}=RE_{\text{inc}}+2RE_F-E_B, \tag{S8}$$

where E_F and E_B are respectively the forward- and back-scattered fields. In the quasi-static approximation, which is reasonable for a typical gold nanorod, E_F and E_B are essentially the same. With the amplitude reflectivity $R\ll 1$, the combined reflected field can be taken to be

$$\begin{aligned} E_{\text{ret}} &\approx RE_{\text{inc}}-E_B \\ &=-\frac{e^{ikr}}{kr}iE_0R\left[1-i\frac{\kappa}{R}\alpha_1\right]\propto 1-i\frac{\kappa}{R}\alpha_1, \end{aligned} \tag{S9}$$

which is also Eq. (2) in the paper.

Quantitative Optical Anisotropy Microscopy

We employ Jones calculus to analyze the optical system. Leaving out the effect of the polarizer, the field after a double-pass transmission through the entire system can be obtained by

$$\mathbb{T}=\mathbf{R}_{-\psi}\mathbf{T}_c\mathbf{R}_{-\varphi}\mathbf{T}_s\mathbf{R}_{\varphi}\mathbf{T}_c\mathbf{R}_{\psi} \tag{S10}$$

where $\mathbf{R}_\varphi$ is a rotation matrix for angle φ around the optical axis, $\mathbf{T_c}$ and $\mathbf{T_s}$ are the Jones matrices for respectively the crystal and the probed GNR, and ψ and φ are the azimuthal angles of the polarizer and the GNR with respect to the slow axis of the birefringent crystal. Each of the constituent matrices can be written in terms of the identity matrix and the SU(2) generating matrices:

$$\mathbf{u_0} = \begin{pmatrix} 1 & 0 \\ 0 & 1 \end{pmatrix}, \mathbf{u_1} = \begin{pmatrix} 0 & i \\ i & 0 \end{pmatrix}, \mathbf{u_2} = \begin{pmatrix} 0 & -1 \\ 1 & 0 \end{pmatrix}, \mathbf{u_3} = \begin{pmatrix} i & 0 \\ 0 & -i \end{pmatrix} \tag{S11}$$

as:

$$\begin{aligned} \mathbf{R}_\varphi &= \begin{pmatrix} \cos\varphi & \sin\varphi \\ -\sin\varphi & \cos\varphi \end{pmatrix} = \cos\varphi \cdot \mathbf{u_0} - \sin\varphi \cdot \mathbf{u_2}, \\ \mathbf{T}_c &= \begin{pmatrix} e^{\frac{ikL_c}{2}} & 0 \\ 0 & e^{-\frac{ikL_c}{2}} \end{pmatrix} = \cos\frac{kL_c}{2}\mathbf{u_0} + \sin\frac{kL_c}{2}\mathbf{u_3}, \\ \mathbf{T}_s &= \begin{pmatrix} c & 0 \\ 0 & c' \end{pmatrix} = a\mathbf{u_0} + b\mathbf{u_3}, \end{aligned} \tag{S12}$$

where k is the wavenumber, L_c is the total birefringence of the crystal, and $a = \frac{c+c'}{2}$ and $b = \frac{c-c'}{2i}$. This notation is useful partly because it simplifies the calculation of $\mathbb{T}$ somewhat, partly because $\{\boldsymbol{u}_i\}$ obey the same algebra as quaternions, which makes it straightforward to implement calculation in software packages that implement quaternions, such as MATLAB and Mathematica. With a bit of work, we then get

$$\begin{aligned} \mathbb{T} = {} & (a\cos kL_c - b\sin kL_c\cos 2\varphi)\cdot\mathbf{u_0} \\ & + \left(a\sin kL_c\sin 2\beta + b(\cos kL_c\sin 2\beta\cos 2\varphi + \cos 2\beta\sin 2\varphi)\right)\cdot\mathbf{u_1} \\ & + \left(a\sin kL_c\cos 2\beta + b(\cos kL_c\cos 2\beta\cos 2\varphi - \sin 2\beta\sin 2\varphi)\right)\cdot\mathbf{u_3} \end{aligned} \tag{S13}$$

The expression for $\mathbf{T}_s$ is sufficiently general to encode the effect of scattering from any non-chiral particle, since the azimuthal orientation of the particle is already accounted for through the $\mathbf{R}_\varphi$ matrices in Eq. (S10). For the case of small nanoparticles like our GNRs, Eqs. (S9) and (2) give us that

$$\begin{cases} c = 1 - \dfrac{i\kappa}{R}\alpha_1 \\ c' = 1 - \dfrac{i\kappa}{R}\alpha_2 \end{cases} \Longrightarrow \begin{cases} a = 1 - \dfrac{i\kappa}{R}\dfrac{\alpha_1 + \alpha_2}{2} = 1 - \dfrac{i\kappa}{2R}\alpha^+ \\ b = \dfrac{\kappa}{2R}(\alpha_2 - \alpha_1) = -\dfrac{\kappa}{2R}\alpha^- \end{cases}. \tag{S14}$$

If we take E_{ref} to be the magnitude of the electric field that reaches the detector with the sample and birefringent crystal removed (but leaving the reflecting substrate), we get that the detected field with sample and all components in place is

$$\boldsymbol{E}_{\mathrm{out}}(k) = \begin{pmatrix}1\\0\end{pmatrix}^T \mathbb{T} \begin{pmatrix}E_{\mathrm{ref}}(k)\\0\end{pmatrix}. \tag{S15}$$

In other words, the effect of the polarizer is to ensure that only light described by $\mathbb{T}_{11}$ reaches the spectrometer. By squaring Eq. (S15), we can write the detected intensity spectrum in terms of $\mathbb{T}$, and also as a sum of terms proportional to multiples of the modulation e^{ikL_c} due to the birefringent crystal: $I_{\mathrm{out}}(k) = I_{\mathrm{ref}}(k)|\mathbb{T}_{11}|^2$, where

$$\begin{aligned} |\mathbb{T}_{11}|^2 = & \begin{bmatrix} |a|^2\left(1 - \frac{1}{2}\sin^2 2\psi\right) + \\ |b|^2\left(\left(1 - \frac{3}{2}\sin^2 2\psi\right)\cos^2 2\varphi + \sin^2 2\psi\right) \end{bmatrix} \\ & + \frac{1}{4}\sin 4\psi \begin{bmatrix} 2i\,\Re\mathrm{e}\{ab^*\}\sin 2\varphi \\ -|b|^2 \sin 4\varphi \end{bmatrix} e^{ikL_c} \\ & + \frac{1}{4}\sin^2 2\psi \begin{bmatrix} 2i\,\Re\mathrm{e}\{ab^*\}\cos 2\varphi + \\ |a|^2 - |b|^2\cos^2 2\varphi \end{bmatrix} e^{2ikL_c} + c.c. \end{aligned} \tag{S16}$$

Two carrier frequencies ($1f$ and $2f$) are thus created in the detected spectrum, corresponding to the single- and double-pass retardation of the crystal (kL_c and $2kL_c$). From Eq. (S14) we have that:

$$|a|^2 = 1 + \frac{\kappa}{R}\alpha_I^+ + \frac{1}{4}\left|\frac{\kappa\alpha^+}{R}\right|^2, \quad |b|^2 = \frac{1}{4}\left|\frac{\kappa\alpha^-}{R}\right|^2,$$
$$\Re\mathrm{e}\{ab^*\} = \frac{\kappa}{2R}\alpha_R^- + \frac{1}{4}\frac{\kappa^2}{R^2}(\alpha_R^-\alpha_I^+ - \alpha_I^-\alpha_R^+). \tag{S17}$$

We will treat this in two limits, at least one of which is likely to be valid for a majority of cases. To simplify the expressions, we choose to take $\psi = \psi_0 = 27.37°$ so that $1 - \frac{3}{2}\sin^2 2\psi_0 = 0$, which is close to the angle used in the actual experiments. Different choices of ψ are certainly possible, but will not change the conclusion of what follows. First, if we are in the weak scattering limit $\frac{\alpha\kappa}{R} \ll 1$, the expression becomes:

$$|\mathbb{T}_{11}|^2 \approx \frac{2}{3} + \frac{1}{2\sqrt{3}}\begin{bmatrix} i\frac{\kappa}{R}\alpha_R^- \sin 2\varphi - \\ -\frac{1}{4}\left|\frac{\kappa\alpha^-}{R}\right|^2 \sin 4\varphi \end{bmatrix} e^{ikL} + \frac{1}{6}\begin{bmatrix} i\frac{\kappa}{R}\alpha_R^- \cos 2\varphi + \\ 1 \end{bmatrix} e^{2ikL} + c.c., \tag{S18}$$

where we are keeping only the leading order of α in each term, as it will be dominant in this limit. Eq. (S18) is then the expression to use for the smallest particles, where only the interferometric and constant terms remain in the expression. In the experiment described in the main paper, we are not quite in this limit, both because the GNRs are relatively strongly scattering near resonance, and because for a glass interface in water $R \approx 0.06$, so that α/κ is actually quite large. Instead, we can use the fact that GNRs are strongly anisotropic, with $\alpha_2 \ll \alpha_1 \Rightarrow \alpha^+ \approx \alpha^- = \alpha_1$. This yields:

$$|\mathbb{T}_{11}|^2 \approx \frac{2}{3}\begin{bmatrix}1+\frac{\kappa\alpha_I}{R}+\\ \frac{5}{12}\left|\frac{\kappa\alpha}{R}\right|^2\end{bmatrix}+\frac{1}{2\sqrt{3}}\begin{bmatrix}i\frac{\kappa}{R}\alpha_R\sin 2\varphi-\\ -\frac{1}{4}\left|\frac{\kappa\alpha}{R}\right|^2\sin 4\varphi\end{bmatrix}e^{ikL}+\frac{1}{6}\begin{bmatrix}i\frac{\kappa}{R}\alpha_R\cos 2\varphi+\\ 1+\frac{\kappa\alpha_I}{R}+\frac{1}{4}\left|\frac{\kappa\alpha}{R}\right|^2\sin^2 2\varphi\end{bmatrix}e^{2ikL}$$

$$+c.c. \tag{S19}$$

Generalizing to the case of arbitrary ψ, the second and third term in this expression lead to Eq. (6) in the main paper. In this limit, terms proportional to α^2 are not negligible, which means that we are able to measure the total scattered light intensity, most conveniently from the real part of the $1f$ term in Eq. (S19). Note however that in the high anisotropy limit, as in the weak scattering limit, the signal is linear in α (or α^-), which is a convenient feature that makes QOAI signals straightforward and convenient to analyze.

Scattering from tilted nanorods

For an arbitrary orientation, the polarization tensor of a nanorod is given by

$$\boldsymbol{\alpha} = \mathbf{A}(\theta,\varphi)^T\begin{pmatrix}\alpha_1 & 0 & 0\\ 0 & \alpha_2 & 0\\ 0 & 0 & \alpha_2\end{pmatrix}\mathbf{A}(\theta,\varphi), \tag{S20}$$

assuming a nanoparticle with its polarizability α_1, α_2 along its principal axes. $\mathbf{A}(\theta,\varphi)$ is the three-dimensional rotation matrix, and θ,φ are the polar and azimuthal angles of the rod. In the calculation of $\mathbb{T}$ in Eq. (S10), it is the top left 2×2 submatrix of the polarization tensor $\boldsymbol{\alpha}$ that enters as:

$$\mathbf{R}_{-\varphi}\mathbf{T}_s\mathbf{R}_{\varphi} = \mathbb{I} - \frac{i\kappa}{R}\boldsymbol{\alpha}_{[1,2;1,2]}. \tag{S21}$$

Since the azimuthal angle φ is already accounted for in Eq. (S10), it therefore suffices to note that $\mathbf{A}(\theta,\varphi) = \mathbf{R}_{\mathrm{y}}(\theta-\pi/2)\mathbf{R}_{\mathrm{z}}(\varphi)$ and that

$$\mathbf{R}_{\mathrm{y}}\left(-\theta+\frac{\pi}{2}\right)\begin{pmatrix}\alpha_1 & 0 & 0\\ 0 & \alpha_2 & 0\\ 0 & 0 & \alpha_2\end{pmatrix}\mathbf{R}_{\mathrm{y}}\left(\theta-\frac{\pi}{2}\right)$$
$$=\begin{pmatrix}\alpha_1\sin^2\theta+\alpha_2\cos^2\theta & 0 & (\alpha_1-\alpha_2)\sin\theta\cos\theta\\ 0 & \alpha_2 & 0\\ (\alpha_1-\alpha_2)\sin\theta\cos\theta & 0 & \alpha_2\sin^2\theta+\alpha_1\cos^2\theta\end{pmatrix}. \quad \text{(S22)}$$

Accordingly, and provided that we are in the high anisotropy limit $\alpha_1 \gg \alpha_2$, the effect of tilting the scattering particle is to make the replacement $\alpha_1 \to \alpha_1 \sin^2\theta$ in Eq. (S14).

Rotational Autocorrelation Functions

For any measured signal X that is a function of a stochastic process $q(t)$, the autocorrelation function of X is:

$$C_X(t) = \langle X[q(t)]X[q(0)]\rangle = \int dq_0 \int dq\, X[q_0]^* X[q]\, p(q_0)p(q,t|q_0), \quad \text{(S23)}$$

where $p(q_0)$ is the unconditional probability density of $q = q_0$ and $p(q,t|q_0)$ is the conditional probability of finding q at time t given q_0 at time $t = 0$. In our case, q will be either the gold nanorod orientation $\Omega = (\theta, \phi)$, or its position $\mathbf{r} = (x, y, z)$. The signals we are measuring are either $d = d_0\big(\boldsymbol{r}(t)\big) \cdot \sin^2\theta(t)$ or $\sin 2\varphi$ (we could also equivalently choose $\cos 2\varphi$).

Following Hinze et al. [3] we have that for the case of our cylindrically symmetric nanorods:

$$p(\Omega_0) = \frac{1}{4\pi}, \quad \text{(S24)}$$
$$p(\Omega, t|, \Omega_0) = \sum_{l,m} Y_l^m(\Omega_0)^*\, Y_l^m(\Omega)\, e^{-l(l+1)D_R t}.$$

$Y_l^m(\Omega)$ are the spherical harmonics and D_R is the rotational diffusivity of the nanorod for rotation around axes perpendicular to the rod. From this, we obtain that

$$C_X(t) = \sum_l A_l e^{-l(l+1)D_R t}, \tag{S25}$$

with

$$A_l = \frac{1}{4\pi} \sum_m \left| \int_0^{2\pi} d\varphi \int_0^{\pi} \sin\theta \, d\theta \, X(\theta, \phi) Y_l^m(\theta, \phi) \right|^2. \tag{S26}$$

For $X = \sin^2\theta$, we obtain:

$$A_l^{(\sin^2\theta)} = \pi \left| \int_0^{\pi} \sin^3\theta \, Y_l^0(\theta, 0) \, d\theta \right|^2, \tag{S27}$$

while for $X = \sin 2\varphi$ (or $\cos 2\varphi$), the coefficients are:

$$A_l^{(\sin 2\varphi)} = A_l^{(\cos 2\varphi)} = \frac{\pi}{2} \left| \int_0^{\pi} \sin\theta \, Y_l^2(\theta, 0) \, d\theta \right|^2. \tag{S28}$$

Due to the symmetry of the spherical harmonics, many of the A_l coefficients are zero. For the $\langle d \rangle$ signal ($X = \sin^2\theta$), only A_0 and A_2 are non-zero, and we have:

$$C_{\sin^2\theta}(t) = \frac{4}{9} + \frac{8}{15} e^{-6D_R t}. \tag{S29}$$

For the orientation measurement ($X = \cos 2\varphi\,, \sin 2\varphi$), $A_0 = 0$ (since we use the range $\varphi \in (-\pi, \pi] \Rightarrow \langle \cos 2\varphi \rangle \equiv 0$), while all other even terms are non-zero. However, the $l = 2$ term dominates the sum, so $C_F(t) \approx C_F(0) e^{-6D_R t}$ is a good approximation, although a better fit can still be obtained by fitting to a stretched exponential [3]. Therefore:

$$C_{\sin 2\varphi}(t) \approx C_{\sin 2\varphi}(0)e^{-\left(\frac{6D_R t}{\alpha}\right)^{\beta}}. \quad \text{(S30)}$$

A nonlinear fit to the series in Eq. (S25) with a cutoff at $l = 22$ yields $\alpha = 0.8285$ and $\beta = 0.8677$.

Estimating the sensitivity of φ measurements

In our 2015 Optics Letter paper [4], we showed that sub-degree angular sensitivity in φ can be achieved in birefringence measurements using our methods. In fact, for sufficiently large phase retardation, the sensitivity can be as high as ~0.01 degrees. To verify that a similar result holds here we cannot rely directly on the plot in Fig. 5(a), since it depends on φ_{SEM}, which is subject to errors that are likely larger than those in φ_{QOAI}. For instance, the image processing algorithm that produces φ_{SEM} from SEM micrographs is of limited precision. There are also systematic errors associated with this measurement due to things like residual astigmatism in the electron optics and rotational misalignment between optical and electron images. It is also likely that there are systematic errors in φ_{QOAI} that do not directly affect the sensitivity of our measurement, for instance due to reflection off the surfaces of the birefringent crystal.

We estimate the sensitivity in φ_{QOAI} for each image used in composing Fig. 5(a) by calculating the standard deviations σ_φ of φ obtained from spectra across each of the spots in the QOAI images underlying the data in Fig. 5. For this calculation we use spectra in

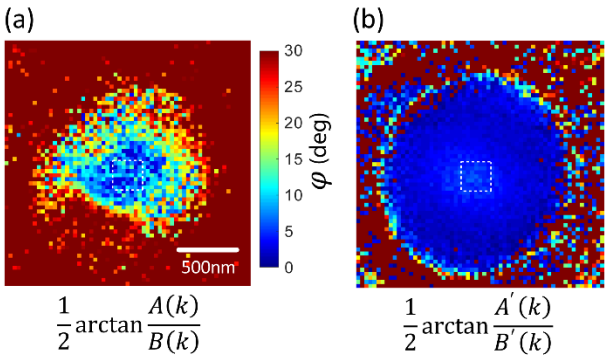

Fig. S2.: *Plots of φ from a single Type II GNR, calculated using (a) the magnitudes of $A(k)$ and $B(k)$, and (b) the slopes of $A(k)$ and $B(k)$. The white dashed boxes delineate the data points used to calculate the σ_φ values plotted in Figs. 5 and S3.*

a 7×7 array centered on the geometric center of each beam spot (see Fig. S2), and that is fully contained within the FWHM of the spot. This involves using data that was taken with a slightly misaligned GNR, and therefore is somewhat suboptimal. The resulting standard deviations are therefore an upper bound on the true sensitivity.

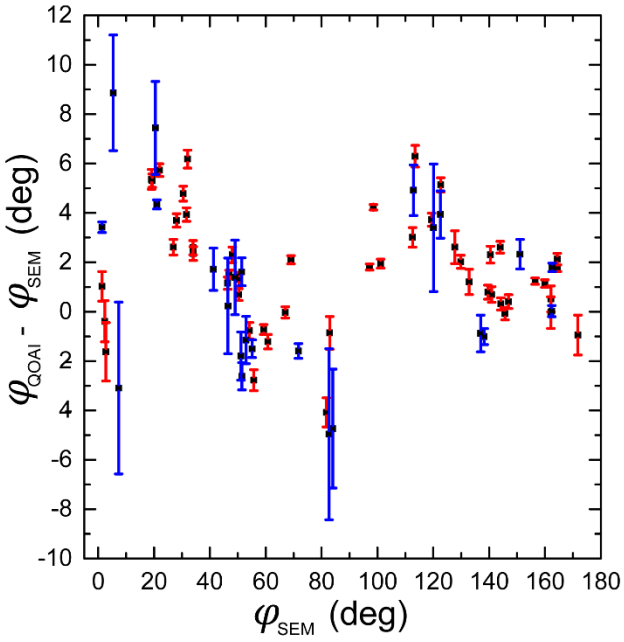

Fig. S3.: *Plot of the residual* $\varphi_{\mathrm{SEM}} - \varphi_{\mathrm{QOAI}}$ *vs* φ_{SEM}. *The error bars indicate the standard deviation in* φ_{QOAI}. *Blue error bars are for Type II particles, while red error bars indicate Type I and III particles.*

This exercise clearly shows why it is important to use Eq. 10 calculate φ for Type II particles. Fig S3 plots the residual $\varphi_{\mathrm{QOAI}} - \varphi_{\mathrm{SEM}}$ and the standard deviation σ_{φ} as in Fig. 5(b), but where we have used Eq. 9 to calculate all values of φ. With few exceptions, σ_{φ} in the Type II particles (blue error bars) is significantly larger in this calculation than in Fig. 5(b). The systematic errors are also bigger in many cases. Fig. S2 illustrates the difference in a different way, by plotting φ for all the spectra collected from a single Type II rod, calculated with respectively Eq. 9 and Eq. 10. The difference is obvious, and we conclude that Eq. 10 is generally superior for finding φ in Type II GNRs.

References

[1] C. F. Bohren, and D. R. Huffman, *Absorption and scattering of light by small particles* (John Wiley & Sons, 2008).
[2] S. Feng, and H. G. Winful, Opt. Lett. **26**, 485 (2001).
[3] G. Hinze, G. Diezemann, and T. Basché, Phys. Rev. Lett. **93**, 203001 (2004).
[4] C. Li, and Y. Zhu, Opt. Lett. **40**, 2622 (2015).